JOURNAL OF CHEMICAL & ENGINEERING DATA

ARTICLE

pubs.acs.org/jced

# Artifical Neural Network (ANN) Modeling and Analysis of Radioactive Gallium-67 Adsorption from Aqueous Solution with Waste Acorns of *Quercus ithaburensis*

Hayrettin Eroglu,*[,†] Mehmet Aktan,[‡] and Gökay Akkaya[‡]

[†]Research Hospital, Nuclear Medicine Discipline, Atatürk University, 25240 Erzurum, Turkey

[‡]Department of Industrial Engineering, Faculty of Engineering, Atatürk University, 25240 Erzurum, Turkey

**ABSTRACT:** The adsorption of gallium-67, which is used in nuclear medicine, was investigated in this study by using waste acorns of *Quercus ithaburensis* (WAQI). The experimental parameters were determined to be as follows: temperature, (283 to 313) K; pH, (2.0 to 10.0); stirring speed, (300 to 720) rpm; particle size, (0.15 to 1.40) mm; and adsorbent dose, (1.0 to 15.0) $g \cdot L^{-1}$. The most effective parameters were pH, temperature, particle size, and adsorbent ratio. The WAQI adsorption mechanism was analyzed by Fourier transform infrared (FTIR) spectra. Adsorption kinetics were studied, and it was seen that WAQI is an excellent Ga-67 adsorbent. An artificial neural network (ANN) was constructed that closely estimates the adsorption amount against temperature, adsorbent ratio, and processing time. The $R^2$ value of the ANN model was 0.997.

## 1. INTRODUCTION

Nuclear medicine uses radioactive materials for diagnosis and treatment. During these processes, radioactive waste is produced. The radioactive waste has harmful effects for the environment. The cancerous influence of radiation is well-known.[1] No body cell is completely resistant against radiation.

After nuclear processes, solid and/or liquid waste is inevitably generated in various activities, concentrations, and chemical forms. Liquid radioactive waste is classified as high activity (more than 10 $Ci \cdot L^{-1}$), medium activity (between ($10^{-2}$ and $10^{-5}$) $Ci \cdot L^{-1}$), low activity (between ($10^{-6}$ and $10^{-9}$) $Ci \cdot L^{-1}$), and very low activity (less than $10^{-9}$ $Ci \cdot L^{-1}$).[2]

The current practice for reducing the harmful effects of radioactive material in nuclear medicine is to keep the liquid waste in waste tanks and the solid waste in lead rooms. These techniques are expensive and impractical and inefficient in radioactivity protection. They require large spaces; they cannot provide good isolation, and they are time-consuming. Finally, radioactive elements may be disposed into the environment before they become stable. Since the radioactive waste also contains metals, they result in metal pollution and even in metal poisoning. When the waste mixes in groundwater, it is more harmful for the environment.[3]

Techniques such as reverse osmosis, ion exchange, settling, and lime coagulation are costly, and they are not effective on low concentrations for toxic metal removal from wastewater.[4] As an alternative to these techniques, bioadsorption can be considered.[5] Many microorganisms such as fungi, yeast, bacteria, and sea organisms can adsorb cationic and anionic materials from water.[6−9] Koshima[10] analyzed the adsorption of thallium(III), gallium(III), gold(III), and iron(III) using AmberliteXAD and Chelex100 resins and presented the findings. Successful results were obtained in the adsorption study of Cr-51 waste, which is also used in nuclear medicine, with the use of water plants named as *Eichhornia crassipes*, *Pistia sp.*, *Nymphaea alba*, *Menhta aquatica*, *Euphorbia sp.*, and *Lemna*.[11] It was shown in many studies that active carbon adsorbs radioactive materials. While Kütahyalı[12] removed uranium with active carbon, Sinha et al.[13] removed radioactive iodine.

In this study, the adsorption of gallium-67 ($^{67}$Ga), which is used for scanning in nuclear medicine, was investigated by using waste acorns of *Quercus ithaburensis* (WAQI).

## 2. MATERIAL AND METHODS

**2.1. Adsorbent.** WAQI is a byproduct of tannin production. The WAQI used in this study was supplied by Salihli Palamut ve Valeks Sanayi TAS in Salihli, Manisa, Turkey. The main components of WAQI are cellulose, hemicelluloses, lignin, some pectin, and extractive materials such as tannin, fatty acids, fatty alcohols, phenols, terpenes, and steroids. WAQI is readily available and inexpensive, and its cost is very low compared to the cost of regeneration. Tannin industry wastes are currently not used for any purpose. Therefore, WAQI does not need to be regenerated.[14] Prior to its use in our experiments, the WAQI was washed with distilled water to remove any impurities. The decolorized and cleaned WAQI was dried at room temperature for a few days. It was then grinded with a strong grinder and sieved to a particle size of (0.15 to 0.30) mm. The Brunauer−Emmett−Teller (BET) surface area, bulk density, and zeta potential (at pH 2) of the biosorbent were determined to be 1.94 $m^2 \cdot g^{-1}$, 0.318 $g \cdot cm^{-3}$, and −5 mV, respectively.

**2.2. Experimental System.** $^{67}$Ga, which is one of the most commonly used radioactive materials in nuclear medicine, was selected to be the material to be adsorbed. It should be known that both its radioactive form and stable form are metal waste, and therefore its purification is important. The radioactive decay

**Received:** September 14, 2010
**Accepted:** March 7, 2011
**Published:** April 02, 2011

ACS Publications © 2011 American Chemical Society

mechanism for $^{67}$Ga is presented in eq 1.

$$^{67}\mathrm{Ga} \rightarrow {}^{67}\mathrm{Zn} + \gamma^{-2}\cdot 93\ \mathrm{keV}(38\ \%) + \gamma^{-3}\cdot 185\ \mathrm{keV}(24\ \%) + \gamma^{-5}\cdot 300\ \mathrm{keV}(16\ \%) + \gamma^{-6}\cdot 394\ \mathrm{keV} \qquad t_{1/2} = 78.25\ \mathrm{h} \tag{1}$$

For the adsorption analysis, 500 mL of purified water was put in a coated reactor, and the pH was adjusted. A pump was connected to the coated reactor to keep the temperature at the desired level. Stirring was performed by a mixer installed to the upper part of the coated reactor. A dosimeter was used to measure the radiation for monitoring the adsorption. This dosimeter takes the liquid from the coated reactor through a pipe, measures the radiation in that pipe's volume, and gives a reference for the radiation in the medium. For isolating from the outer medium, this dose calibrator was covered with lead, and the only opening was for the pipe. The tip of the pipe inside the coated reactor was covered with a filter that does not adsorb radioactive materials and prevents the passage of solid adsorbents. The amount used in the experiments was equal to the amount given to patients, and the rate of urination was considered in the measurements. Parameters used in the experiments were temperature, pH, stirring speed, adsorbent ratio, and particle size.

**2.3. Preparation of the Radioactive Solution.** Experiments were conducted on the same days of the week considering the activity of $^{67}$Ga and calibration date. At the calibration date and time, the activity of gallium was 37 MBq·mL$^{-1}$ and had 99 % radionuclide purity. An average of 500 $\mu$Ci of $^{67}$Ga was used in 500 mL solutions for the experiments. Temperature, pH, and stirring speed of the solutions were adjusted, and the adsorbent was added for attaining stability. Finally, $^{67}$Ga was added inside the stable solution for conducting the experiments.

**2.4. The Zeta Potential.** The zeta potential of the adsorbent was measured by a zeta meter (ZETAMETER 3.0 + 542). The measurements were taken for the conditions of covering the pH values of the present adsorption studies at an adsorbent dose of 10 (kg adsorbent)·m$^{-3}$ pure water and room temperature. Before the measurements, the adsorbent-solution medium was well-stirred for about 10 min for homogenization. For pH adjustment in the measurements, HCl and NaOH solutions were used.

**2.5. Fourier Transform Infrared (FTIR) Spectroscopy.** Fourier transform infrared (FTIR) spectroscopy studies were also performed for the characterization of the adsorption mechanism of $^{67}$Ga on WAQI. The FTIR spectra were obtained using a Perkin-Elmer Spectrum One FTIR spectrometer.

## 3. RESULTS AND DISCUSSION

The base values for the parameters were 2 for the pH, 293 K for the temperature, 10 g·L$^{-1}$ for the adsorbent ratio, 600 rpm for the steering speed, and (0.15 to 0.30) mm for the particle size. It was assumed that the adsorption was stabilized in 120 min, and the following results were obtained.

**3.1. Effects of Experimental Parameters.** Selected levels for the starting pH were 2, 4, 6, 7, 8, and 10. Figure 1a presents the $^{67}$Ga removal rate versus pH. It is seen that the highest $^{67}$Ga removal rate was attained when the pH was 2. It can be seen in Figure 1a that 82.4 % of $^{67}$Ga can be removed in 120 min when the pH is 2. The starting pH was set to 2.0 since the highest adsorption of $^{67}$Ga was attained at that pH level.

The hydrolysis of $Ga^{3+}$ is very fast in an aqueous environment. Chemical reactions related to the hydrolysis of $Ga^{3+}$ in water are as follows:[15]

$$[\mathrm{Ga}]^{3+} + \mathrm{H_2O} = [\mathrm{Ga(OH)}]^{2+} + \mathrm{H^+} \tag{2}$$

$$[\mathrm{Ga(OH)}]^{2+} + \mathrm{H_2O} = [\mathrm{Ga(OH)_2}]^{+} + \mathrm{H^+} \tag{3}$$

$$[\mathrm{Ga(OH)_2}]^{+} + \mathrm{H_2O} = [\mathrm{Ga(OH)_3}] + \mathrm{H^+} \tag{4}$$

$$[\mathrm{Ga(OH)_3}] + \mathrm{H_2O} = [\mathrm{Ga(OH)_4}]^{-} + \mathrm{H^+} \tag{5}$$

In an aqueous environment, $[\mathrm{Ga}]^{3+}$ ions and some $[\mathrm{Ga(OH)}]^{2+}$ ions are present at pH 2. Since the zeta potential of the adsorbent at pH 2 is −5 mV, positively charged Ga ions are adsorbed by interacting with the negatively charged adsorbent. As the pH increases to 10, $Ga(OH)_3$ is converted to $[Ga(OH)_4]^-$ by interacting with $OH^-$ ions in the aqueous environment. At increasing pH, gallium forms various gallium hydroxide species, of which the first one is neutral and the others are negatively charged compounds. Therefore, as pH increases, bioadsorption decreases due to the depletion effect of repulsion between the negative charges of gallium hydroxide species and the bioadsorbent surface. Consequently, this behavior indicates that the process mainly occurs due to chemical adsorption.[15,16]

The tested stirring speeds were (360, 480, 600, and 720) rpm. Figure 1b presents the $^{67}$Ga removal rate versus stirring speed. It was shown that the highest $^{67}$Ga removal rate was obtained at 720 rpm. When the stirring speed increased, Ga ions can reach solid particles more easily. Considering the economy and the facts that there is not a big difference in removal rate when the stirring speed is changed and particles can be uniformly diffused at 600 rpm, the stirring speed for the experiments was selected to be 600 rpm.

The WAQI particle size levels for $^{67}$Ga adsorption were set as (0.15 to 0.30) mm, (0.30 to 0.70) mm, and (0.70 to 1.4) mm. Figure 1c presents the $^{67}$Ga removal rate versus WAQI particle size. The highest $^{67}$Ga adsorption rate in 120 min was 82.4 % when the WAQI particle size was set to (0.15 to 0.30) mm. A higher efficiency is an expected result when the surface area increases with a smaller particle size.

Experimental medium temperature levels were 283 K, 293 K, 303 K, and 313 K. The resulting $^{67}$Ga removal rates are given in Figure 1d. The highest $^{67}$Ga adsorption rate in 120 min was 90.0 % when the temperature was set to 313 K. Temperature is one of the most effective parameters on the adsorption. Increasing adsorption with increasing temperature gives rise to the thought that adsorption has a chemical character.

Adsorbent ratio levels in 1 L of liquid were 1 g, 2.5 g, 5 g, 10 g, and 15 g solid WAQI, and temperature levels were 283 K, 293 K, 303 K, and 313 K. As can be seen in Figure 1e, a higher adsorbent ratio and temperature result in higher adsorption in 120 min.

**3.2. Thermodynamic Analysis.** The distribution coefficient can be calculated as

$$k_D = C_{\mathrm{adsorbed}}/C_{\mathrm{non\text{-}adsorbed}} \tag{6}$$

$\Delta G$ can be calculated from the following equation:

$$\Delta G = -RT \ln k_D \tag{7}$$

Since

$$\Delta G = \Delta H - T\Delta S \tag{8}$$

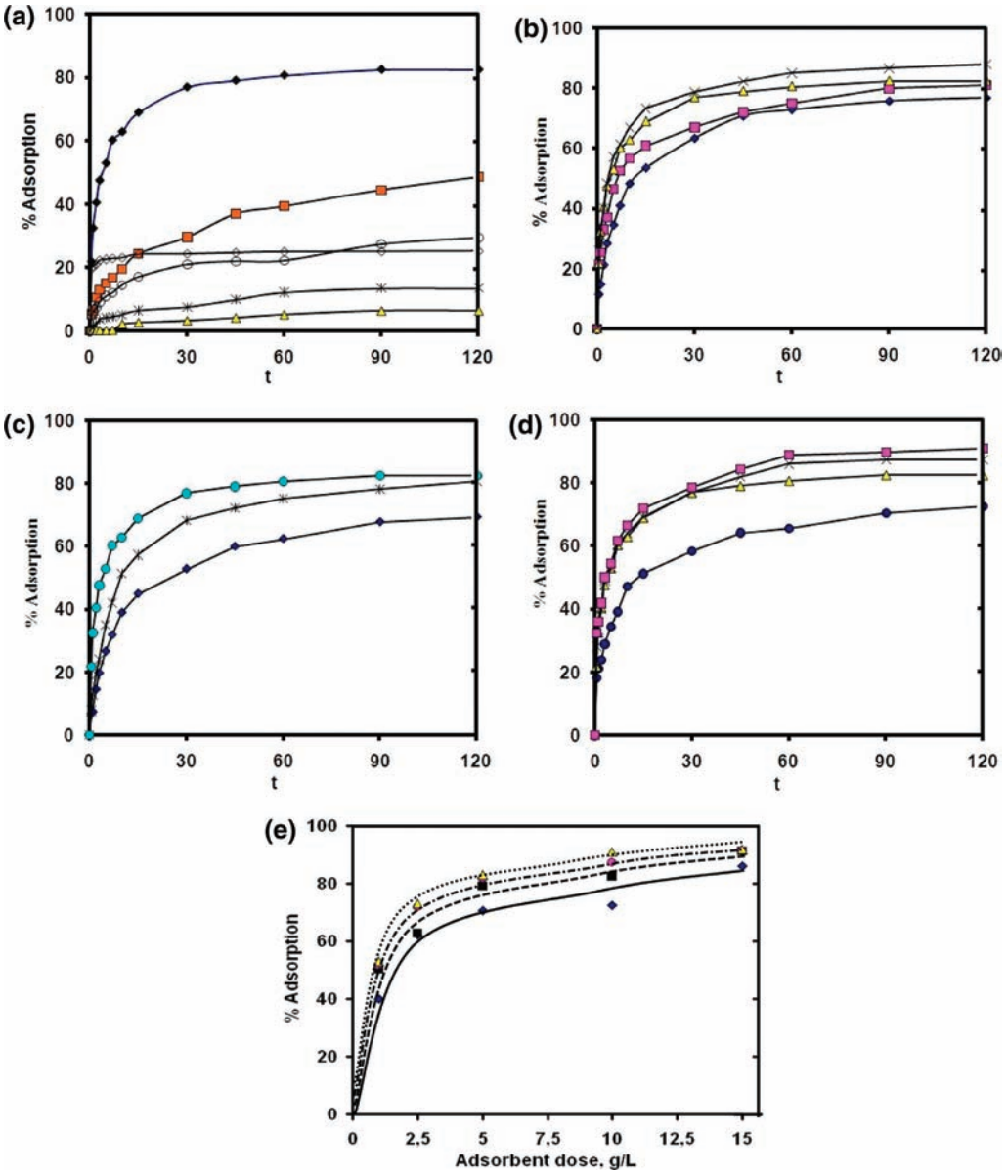


**Figure 1.** (a) Adsorption vs pH; ♦, pH 2; ■, pH 4; ×, pH 6; △, pH 7; ○, pH 8; ◇, pH 10. (b) Adsorption vs stirring speed; ♦, 360 rpm; ■, 480 rpm; △, 600 rpm; ×, 720 rpm. (c) Adsorption vs particle size; ○, (0.15 to 0.3 mm); ×, (0.3 to 0.7 mm); ♦, (0.7 to 1.4 mm). (d) Adsorption vs temperature; ●, 283 K; △, 293 K; ×, 303 K; ■, 313 K. (e) Adsorption vs adsorbent ratio; ♦, 283 K; ■, 293 K; ●, 303 K; △, 313 K.

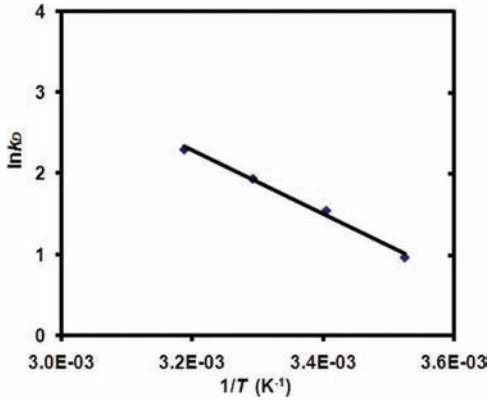


**Figure 2.** Plot of ln $k_D$ versus $1/T$.

eq 9 can be obtained by using eqs 7 and 8 as

$$\ln k_D = \frac{\Delta S}{R} - \frac{\Delta H}{RT} \quad (9)$$

where $k_D$ is the distribution coefficient, $\Delta G$ is the Gibbs energy change ($J \cdot mol^{-1}$), $\Delta H$ is the enthalpy change ($J \cdot mol^{-1}$), $R$ is the universal gas constant (8314 $J \cdot K^{-1} \cdot mol^{-1}$), $\Delta S$ is the entropy change ($J \cdot mol^{-1} \cdot K^{-1}$), and $T$ is the absolute temperature in Kelvin (K).

$\Delta H$ and $\Delta S$ can be found when a plot of $1/T$ against ln $k_D$ is drawn, as given in Figure 2.[12,16] $\Delta G$ values for several temperatures were calculated by using eq 8, and they are provided in Table 1.

For this process, $\Delta H$ and $\Delta S$ were found to be 32.524 $kJ \cdot mol^{-1}$ and $-0.123$ $kJ \cdot mol^{-1} \cdot K^{-1}$, respectively. The negative $\Delta G$ implies that the adsorption will occur spontaneously,

and the positive $\Delta H$ implies that the adsorption is endothermic and the efficiency increases with increasing temperature. All of these findings give rise to the thought that the adsorption has a chemical character.

**3.3. FTIR Analysis of WAQI.** FTIR spectra were taken before and after the adsorption for determining the functional groups active on $^{67}$Ga removal using WAQI. Changes (especially reductions) observed in the FTIR spectra after the adsorption imply that the active groups take part in the biosorption.

Figure 3 shows 13 adsorption bands that are present in the complex structure of the adsorbent. These are the complex adsorption band characteristics of the WAQI.

Table 2 sorts the most important eight bands of the functional groups over the waste in decreasing order. These bands are (3922, 3610, 3532, 3310, 3206, 2139, 1054, and 556) $cm^{-1}$. Effective groups in order were OH, N−H stretching, C−O stretching of ether groups, and C−C groups according to the spectrum analysis

**Table 1. Values of $\Delta G$ at Different Temperatures**

| temperature, K | 283 | 293 | 303 | 313 |
|---|---|---|---|---|
| $\Delta G$, kJ·mol$^{-1}$ | −2.275 | −3.770 | −4.891 | −6.003 |

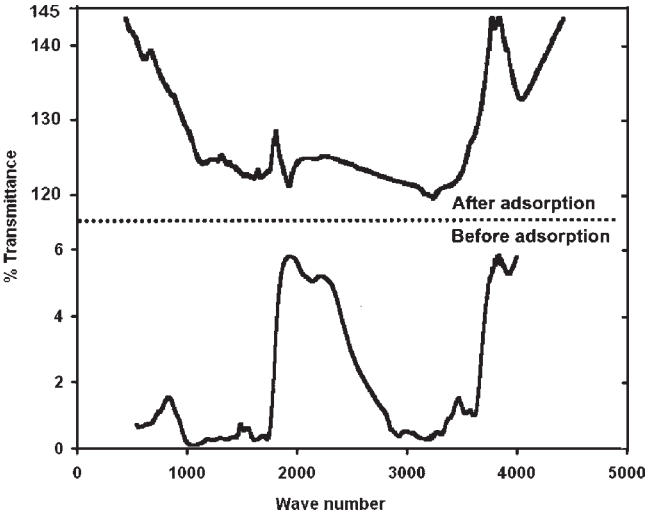


**Figure 3.** FTIR spectra of WAQI before and after adsorption.

of gallium before and after adsorption. These groups are very effective on the adsorption, and the adsorption occurs fast with these groups. Gallium can interact with these functional groups and can form a complex. The amount of 82.4 % of $^{67}$Ga can be adsorbed in 120 min with WAQI when the pH is 2. These results show that metal ions form good bonds with the adsorbent.

**3.4. Kinetics of the Adsorption.** Models of adsorption kinetics are related to the removal rate of the adsorbent. These models are necessary for the planning of recycling processes by adsorption. Pseudofirst-order, pseudosecond-order, and Elovich kinetic models are the three main reaction models. Equations for these models are given in Table 3.

In Table 3, $h$ is the initial adsorption rate, $t$ is the adsorption period (min), $k$ is the kinetic rate constant, $\alpha$ is the Elovich coefficient (the initial sorption rate (mg·g$^{-1}$·min$^{-1}$)), $\beta$ is the Elovich coefficient (desorption constant (g·mg$^{-1}$)), $q_e$ is the adsorbed amount per amount adsorbent at equilibrium (mg·g$^{-1}$), and $q_t$ is the adsorbed amount per amount adsorbent at any time (mg·g$^{-1}$).[17,18]

It was seen that the adsorption occurs very fast, and the effective parameters are temperature, pH, particle size, and the adsorbent ratio. The adsorption efficiency increases with increasing temperature. All kinetic models were tested, and the best fitting model was found to be the pseudosecond-order model. Calculated values are given in Table 4. Their regression coefficients are all high except for the ones for pH = 6 and pH = 7. Table 4 shows that experimental values and the theoretical values are very close to each other in the pseudosecond-order model. Such a result implies that the pseudosecond-order model is a good fit. The Elovich kinetic model also well represents the kinetic data. This can indicate that chemisorption had an important role in this process because this model is in good agreement with the data of chemisorption processes.

**3.5. Adsorption Mechanism.** Usually there are three consecutive steps in an adsorption process. These are film diffusion, intraparticle or pore diffusion, and sorption to inner regions. The last of these three steps can be omitted since it is fairly fast. The slowest of either the film diffusion or pore diffusion steps will be the one that controls the process.[19] Weber and Morris stated that the adsorbed amount ($q_t$) is proportional to the square root of time if the controlling step is pore diffusion. The Weber and

**Table 2. FTIR Spectral Characteristics of WAQI before and after Adsorption**

| | frequency ($cm^{-1}$) | | | |
|---|---|---|---|---|
| IR peak | before ads. | after ads. | differences | assignment |
| 1 | 3922 | 3652 | −270 | bonded −OH groups |
| 2 | 3610 | did not appear | unknown | bonded −OH groups |
| 3 | 3532 | 3436 | −96 | bonded −OH groups |
| 4 | 3310 | 3244 | −66 | bonded −OH groups |
| 5 | 3206 | did not appear | unknown | N−H stretching |
| 6 | 2922 | 2922 | 0 | aliphatic C—H group |
| 7 | 2139 | did not appear | unknown | C≡N stretching |
| 8 | 1730 | 1735 | +5 | C═O stretching |
| 9 | 1614 | 1618 | +4 | C═N stretching |
| 10 | 1511 | 1511 | 0 | secondary amine group |
| 11 | 1454 | 1454 | 0 | symmetric bending of $CH_3$ |
| 12 | 1054 | 1026 | −28 | C—O stretching of ether groups |
| 13 | 556 | did not appear | unknown | −C—C− group |


dx.doi.org/10.1021/je100929z |J. Chem. Eng. Data 2011, 56, 1910–1917

**Table 3. Kinetic Equations Used for Analysis of Kinetic Data**[16]

| kinetic equation | linear form of equation | plot |
|---|---|---|
| pseudofirst order | $\ln(q_e - q_t) = \ln q_e - kt$ (10) | $\ln(q_e - q_t)$ versus $t$ |
| pseudosecond order | $(t/q_t) = 1/(kq_e^2) + (1/q_e)t$ (11) | $t/q_t$ versus $t$ |
| | $h = kq^2$ (12) | |
| Elovich | $q_t = (1/\beta)\ln(\alpha\beta) + (1/\beta)\ln t$ (13) | $q_t$ versus ln$t$ |

**Table 4. Fit of Experimental Data with Pseudosecond-Order Kinetic Model for Experimental Parameters**

| kinetic models | | pseudofirst-order kinetic models | | | pseudosecond-order kinetic model | | | | | Elovich equation | | |
|---|---|---|---|---|---|---|---|---|---|---|---|---|
| parameters | | $R^2$ | $k$ | $q(\text{thr})\cdot 10^6$ | $R^2$ | $kx\cdot 10^{-4}$ | $h\cdot 10^6$ | $q(\text{thr})\cdot 10^6$ | $q(\text{exp})\cdot 10^6$ | $R^2$ | $\beta\cdot 10^{-6}$ | $\alpha\cdot 10^6$ |
| temperature (K) | 283 | 0.963 | 0.0357 | 4.030 | 0.9961 | 3.544 | 1.349 | 6.169 | 6.082 | 0.981 | 1.11 | 8.31 |
| | 293 | 0.938 | 0.0588 | 3.664 | 0.9995 | 6.649 | 3.035 | 6.756 | 6.641 | 0.974 | 1.11 | 25.2 |
| | 303 | 0.958 | 0.0589 | 4.57 | 0.9988 | 4.916 | 2.886 | 7.662 | 7.516 | 0.988 | 1.00 | 20.1 |
| | 313 | 0.957 | 0.0465 | 4.506 | 0.9986 | 4.443 | 3.005 | 8.224 | 8.108 | 0.988 | 1.00 | 20.1 |
| pH | 2 | 0.938 | 0.0588 | 4.030 | 0.9995 | 6.649 | 3.035 | 6.756 | 6.641 | 0.974 | 1.11 | 25.2 |
| | 4 | 0.986 | 0.0257 | 3.349 | 0.9763 | 2.294 | 0.388 | 4.114 | 4.026 | 0.950 | 1.43 | 1.24 |
| | 6 | 0.946 | 0.0328 | 0.954 | 0.7131 | 3.087 | 0.0509 | 1.284 | 1.045 | 0.942 | 5.00 | 0.257 |
| | 7 | 0.965 | 0.0271 | 0.638 | 0.2448 | - | - | - | 0.621 | 0.86 | 10.0 | 0.201 |
| | 8 | 0.94 | 0.0249 | 1.924 | 0.9793 | 5.1 | 0.322 | 2.514 | 2.532 | 0.962 | 2.50 | 1.09 |
| | 10 | 0.831 | 0.0476 | 0.408 | 0.9999 | 8.343 | 4.341 | 2.281 | 2.278 | 0.967 | 11.1 | 8.31 |
| stirring speed (RPM) | 360 | 0.983 | 0.0453 | 4.525 | 0.9973 | 3.013 | 1.226 | 6.169 | 6.16 | 0.987 | 1.00 | 2.72 |
| | 480 | 0.957 | 0.0409 | 4.556 | 0.9995 | 6.648 | 3.034 | 6.379 | 7.339 | 0.991 | 1.00 | 7.39 |
| | 600 | 0.938 | 0.0588 | 4.030 | 0.9995 | 6.649 | 3.035 | 6.756 | 6.641 | 0.974 | 1.11 | 25.2 |
| | 720 | 0.929 | 0.0430 | 3.675 | 0.9992 | 5.651 | 2.975 | 6.756 | 7.181 | 0.976 | 1.00 | 20.1 |
| particle size (mm) | 1.40 to 0.70 | 0.957 | 0.0379 | 4.951 | 0.9946 | 2.16 | 0.780 | 7.256 | 5.738 | 0.985 | 1.11 | 25.2 |
| | 0.70 to 0.30 | 0.945 | 0.0443 | 4.575 | 0.9975 | 2.487 | 1.148 | 6.008 | 7.181 | 0.982 | 1.00 | 2.72 |
| | 0.30 to 0.15 | 0.938 | 0.0588 | 4.030 | 0.9995 | 6.649 | 3.035 | 6.794 | 6.641 | 0.974 | 1.00 | 2.01 |

Morris equation is as follows:[20]

$$q_t = k_i\sqrt{t} + Z \quad (14)$$

where $k_i$ is the intraparticle diffusion coefficient ($\text{mg}\cdot\text{g}\cdot\text{s}^{0.5}$). The diffusion coefficient is strongly related to surface features of the adsorbent. The diffusion coefficient for adsorption can be calculated as[21,22]

$$f\left(\frac{q_t}{q_e}\right) = -\log\left[1 - \left(\frac{q_t}{q_e}\right)\right] = \frac{\pi^2 Dt}{2.3{r_o}^2} \quad (15)$$

If the rate process is considered to be pseudosecond-order, then;[18]

$$t_{1/2} = \frac{1}{k\cdot q_e} \quad (16)$$

When the half-life period is put into the equation, it can be seen that

$$t_{1/2} = \frac{0.030{r_0}^2}{D} \quad (17)$$

where $D$ is the diffusion coefficient ($\text{cm}^2\cdot\text{s}^{-1}$) and $r_0$ is the radius of the adsorbent particle (cm).

High correlation coefficients in the intraparticle diffusion results imply that the adsorption process is controlled by intraparticle diffusion.

Therefore, it can be concluded that the controlling step is the diffusion through the pores in the particle. It can be seen in Table 5 that the diffusion coefficient is largest for pH 2. The reason for small diffusion coefficients with other pH values is less adsorption at those pH values. The diffusion coefficient increases as the temperature increases since the adsorption rate becomes larger with increasing temperature. All of these results show that the adsorption mechanism is controlled by the intraparticle diffusion process.

**3.6. Artificial Neural Network (ANN) Model.** The use of artificial neural networks (ANNs) in medicine is increasing in areas such as drug research and development, disease diagnosis and prognosis, and survival analysis. A steady increase in the number of publications concerning ANNs in medicine has been seen in the past decade. Many of these demonstrate that neural networks offer equivalent if not superior performance when compared with other statistical methods in several areas of medicine.[23]

An ANN makes possible the definition of the relation (linear or nonlinear) among a number of variables without knowledge of their cause-effect mechanisms. One of the main functions of ANNs is their excellent ability to model a complex multiinput multioutput system.[24] A multilayer perceptron (MLP)

is composed of multiple neurons arranged in several different layers. The configuration of the best MLP model includes choosing the number of layers, the number of neurons in hidden layer(s), the activation function, the error function, and the learning algorithm. After the proper architecture of the MLP has been established, all of the training cases are run through the network. In each neuron, a linear combination of the weighted inputs (including a bias) is computed, summed, and transformed using a transfer function (linear or nonlinear). The value obtained is passed on as an input to the neurons in the subsequent layer until a value is computed in neurons of the output layer. The output values are compared with the target outputs. The difference between the output and the target is calculated using a certain error function to give the prediction error made by the network. Then, the training algorithm is used to adjust the network's weights and thresholds to minimize this error.[25,26]

In this study, a hyperbolic tangent function was used in hidden layer neurons, and a logistic function was used in output layers. Networks were trained using the back-propagation algorithm. Weighted sums of the input components are calculated by using the following function:

$$u_j = \sum_{i=1}^{n} w_{ij}x_i - b_j \tag{18}$$

where $u_j$ is the weighted sum of the $j$th neuron for the input received from the preceding layer with $n$ neurons, $w_{ij}$ is the weight between the $j$th neuron and the $i$th neuron in the preceding layer, $x_i$ is the output of the $i$th neuron in the preceding layer, and $b_j$ is the bias of the $j$th neuron. The output of the $j$th neuron $a_j$ in a hidden layer is calculated with a hyperbolic tangent function as

$$a_j = f(u_j) = \frac{\exp(u_j) - \exp(-u_j)}{\exp(u_j) + \exp(-u_j)} \tag{19}$$

and the outputs of the output layer is calculated with a logistic function as

$$a_j = f(u_j) = \frac{1}{1 + \exp(-u_j)} \tag{20}$$

The technique consists of subdivided data sets in three subsets: training (approximately two-thirds of total data), validation (one-sixth of total data), and test (one-sixth of total data). The best network was searched using one-hidden layer and two-hidden layer network architectures. A minimum test-set error

**Table 5. Calculations of the Intraparticle Model**

| parameters | | $t_{1/2}$ | $k_i \cdot 10^7$ | $D \cdot 10^6$ | $R^2$ |
|---|---|---|---|---|---|
| temperature (K) | 283 | 4.64 | 5 | 3.27 | 0.902 |
| | 293 | 2.27 | 4 | 6.71 | 0.771 |
| | 303 | 2.71 | 5 | 5.61 | 0.837 |
| | 313 | 2.78 | 5 | 5.47 | 0.857 |
| pH | 2 | 2.27 | 4 | 6.71 | 0.771 |
| | 4 | 10.83 | 4 | 1.40 | 0.980 |
| | 6 | 31 | 1 | 0.49 | 0.965 |
| | 7 | - | 0.7 | - | 0.955 |
| | 8 | 77.44 | 2 | 0.20 | 0.959 |
| | 10 | 5.26 | 0.4 | 2.88 | 0.771 |

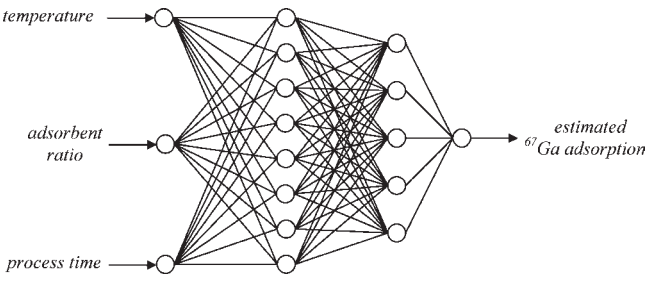


**Figure 4.** Selected ANN architecture.

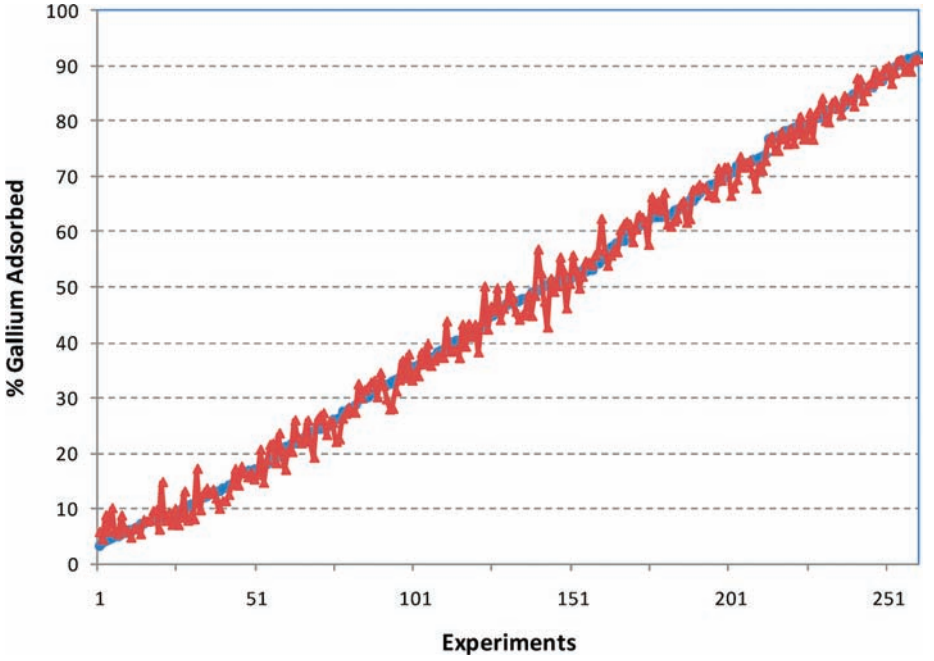


**Figure 5.** ANN estimates and actual $^{67}$Ga adsorption data; ▲, estimates; ●, actual data.


dx.doi.org/10.1021/je100929z |J. Chem. Eng. Data 2011, 56, 1910–1917

criterion was used for selecting the number of hidden layers and number of neurons in each layer. The Levenberg−Marquardt optimization technique was implemented for error minimization by adjusting network weights.[27] To prevent overfitting problems, early stopping conditions were adopted.

Input variables of the ANN were temperature (four levels: 283 K, 293 K, 303 K, and 313 K), adsorbent ratio (five levels: 1 g·L$^{-1}$, 2.5 g·L$^{-1}$, 5 g·L$^{-1}$, 10 g·L$^{-1}$, and 15 g·L$^{-1}$ of solid WAQI), and time (13 levels: 0.5 min, 1 min, 2 min, 3 min, 5 min, 7 min, 10 min, 15 min, 30 min, 45 min, 60 min, 90 min, and 120 min). So, the number of experimental runs for constructing the ANN was $4 \times 5 \times 13 = 260$. The output to be estimated by the ANN was the adsorbed percent of $^{67}$Ga.

Figure 4 shows the network structure that minimized the test-set sum of squared errors. The selected ANN has eight neurons in the first hidden layer and five neurons in the second hidden layer.

The $R^2$ value ($0 \le R^2 \le 1$) of a model is the proportion of the total variability in the dependent variable that is accounted for by the model.[28] An $R^2$ value ($R^2 = 1$ implies perfect matching of predicted and actual data) of the ANN model is a measure of its estimation performance for the actual observed values. We noted that the $R^2$ value of the ANN model was approximately 0.997, which means that the ANN closely predicts the $^{67}$Ga adsorption since $R^2$ is very close to 1. Figure 5 is the plot of the estimated $^{67}$Ga adsorption against observed (target) adsorption values in increasing order, which also presents the close predictions of the ANN model.

## 4. CONCLUSIONS

This study investigated the adsorption of a radioactive metal from liquid waste using WAQI as a biosorbent. Successful results were obtained with WAQI as an adsorbent. Adsorption was stabilized within 120 min with a high adsorption rate. Ideal conditions for adsorption were found to be 600 rpm for the stirring speed, (0.15 to 0.30) mm for particle size, 293 K for medium temperature, pH 2 for medium pH, and 15 g·L$^{-1}$ for the solid/liquid ratio. Because of economic concerns, a low stirring speed and temperature may be selected. With a starting radioactive concentration of 500 $\mu$Ci, 91.8 % of $^{67}$Ga was adsorbed under the ideal adsorption conditions mentioned above. It is thought that the adsorption has an endothermic and chemical character. FTIR spectra were analyzed, and it is thought that the adsorption is physicochemical and has a complex structure with multiple mechanisms. The adsorption kinetics fit a pseudosecond-order model. The analysis also shows that the bioadsorption mechanism is controlled by intraparticle or pore diffusion processes.

Current regulations in Turkey are in accordance with the International Atomic Energy Agency and put a yearly limit of 1 $\mu$Ci which is the radiation dose to be emitted to the environment. Urinary or unused $^{67}$Ga output requires a waiting time of (10 to 22) weeks for nuclear medicine centers before they dispose the waste to the environment. Since the radioactive output of such centers accumulates every week, the current technique of keeping the waste in lead tanks is expensive and inefficient. At the same time, since $^{67}$Ga decays to $^{67}$Zn, the latter is still harmful in disposal due to poisoning and pollution effects.

Results show that adsorption prevents the harmful effects of such radioactive materials for the environment. Since the stable forms of radioactive metals are still harmful metals, adsorption also prevents such effects with an economic solution. It was seen that nearly 92 % of $^{67}$Ga in 1 m$^3$ of liquid waste can be adsorbed with 1.5 kg of adsorbent. Optimal adsorption conditions of WAQI for other radioactive materials can also be determined. Since the WAQI itself is also a waste, the adsorption process prevents the disposal of both radioactive and solid wastes, can support their recycling, and benefit the economy.

Mathematically defined adsorption equations of $^{67}$Ga with WAQI are not available, and the adsorption process is influenced by multiple variables. Since ANNs make possible the definition of the relation (linear or nonlinear) among a number of variables without knowledge of their cause and effect mechanisms, the application of an ANN is appropriate for estimating the adsorbed rate of $^{67}$Ga and determining the optimal levels of input parameters for maximum adsorption of $^{67}$Ga. So, the ANN can model the nonlinear relationship between the adsorption rate and the controllable input variables. An ANN model was constructed using the experimental data. The adsorption rate of the radioactive material was estimated with the ANN, and the optimal conditions for maximum adsorption were determined by using the ANN model. The $R^2$ value of the ANN model was 0.997, which means that the estimates of the constructed ANN are very close to the actual $^{67}$Ga adsorption observations.

## AUTHOR INFORMATION

### Corresponding Author

*E-mail: heroglu@atauni.edu.tr. Tel.: +90 442 231 4553. Fax: +90 442 231 4544.

## REFERENCES

(1) Görpe, A.; Cantez, S. *Practical Nuclear Medicine*; İstanbul Medical School Foundation: Istanbul, 1992.

(2) Marinin, D. V.; Brown, G. N. Studies of sorbent/ion-exchange materials fort the removal of radioactive strontium from liquid radioactive waste and high hardness groundwaters. *Waste Manage.* **2000**, *205*, 545–553.

(3) Eroglu, H. *Adsorption of Radioactive Thallium-201 and Gallium-67 that are Used in Nuclear Medicine*; Atatürk Üniversity Graduate School:
Erzurum, 2009.

(4) Dean, J. G.; Bosqui, F. L.; Lanoutte, K. H. Heavy metals from waste waters. *Environ. Sci. Technol.* **1972**, *6*, 518–524.

(5) Volesky, B. *Bio-sorption and Bio-sorbents. Bio-sorption of Heavy Metals*; CRC Press: Boca Raton, FL, 1990.

(6) Luef, E.; Thedor, P.; Christian, P. K. Adsorbtion of zinc by fungal mycelial wastes. *Appl. Microbiol. Biotechnol.* **1991**, *34*, 688–692.

(7) McLean, R. J. C.; Campbell, A. M.; Khu, P. T.; Persaud, A. T.; Bickerton, L. E.; Chemin, D. Repeated use of *Bacillus subtilis* cell walls for copper binding. *J. Microbiol. Biotechnol.* **1994**, *10*, 472–474.

(8) Volesky, B.; Holan, Z. R. Adsorbtion of heavy metals. *Biotechnol. Prog.* **1995**, *11*, 235–250.

(9) Volesky, B.; May-Philips, H. A. Adsorbtion of heavy metals by Saccharomyces cerevisiae. *Appl. Microbiol. Biotechnol.* **1995**, *42*, 797–806.

(10) Koshima, H. Adsorption of Iron(III), Gold(III), Gallium(III), Thallium(III) and Antimony(V) on Amberlite XAD and Chelex 100 resins from hydrochloric acid solution. *Anal. Sci.* **1986**, *2*, 225–260.

(11) Taner, S. T.; Demirel, Z.; Üst, Z. *An Adsorbent Proposal that can be Used for Cr-51 Waste of Medical Field*; Ege Üniversity Graduate School: Izmir, 2003.

(12) Kütahyalı, C. *Analysis of Selective Adsorption and Application Fields of Uranium by Using Active Carbon Produced from Charcoal*; Ege Üniversity Graduate School: Izmir, 2002.

(13) Sinha, P. K.; Lal, K. B.; Ahmed, J. Removal of radioiodine from liquid effluents. *Waste Manage.* **1997**, *17*, 33–37.

(14) Bozkurt, A. Y.; Yaltirik, F.; Ozdonmez, M. *Forest By-products in Turkey*; Istanbul University: Istanbul, 1982.
(15) Jackson, E. G.; Byrne, M. J. Metal Ion Speciation in Blood Plasma: Gallium-67-Citrate and MRJ Contrast Agent. *J. Nucl. Med.* **1996**, *37*, 379–386.
(16) Eroglu, H.; Varoglu, E.; Yapici, S.; Sahin, A. An environmentally friendly batch bioadsorption study of the radionuclides $^{67}$Ga from aqueous solutions by fibrous tea waste. *Chem. Eng. J.* **2010**, *165*, 563–572.
(17) Vinod, K. G.; İmran, A. Removal of Endosulfan and Methoxychlor from Water on Carbon Slurry. *Environ. Sci. Technol.* **2008**, *42*, 766–770.
(18) Alkan, M.; Doğan, M.; Turhan, Y.; Demirbaş, Ö.; Turan, P. Adsorption kinetics and mechanism of maxilon blue 5G dye on sepiolite from aqueous solutions. *Chem. Eng. J.* **2008**, *139*, 213–223.
(19) Ho, Y. S.; McKay, G. Sorption of dye from aqueous solution by peat. *Chem. Eng. J.* **1998**, *70*, 115–124.
(20) Weber, W. J.; Morris, J. C.; Sanit, J. Kinetics of adsorbtion on carbon from solution. *Eng. Div.* **1963**, *89*, 31–39.
(21) Kavitha, D.; Namasivayam, C. Experimental and kinetic studies on methylene blue adsorbtion by coir pith carbon. *Bioresour. Technol.* **2007**, *98*, 14–21.
(22) Wang, B. E.; Hu, Y. Y.; Xie, L.; Peng, K. Biosorption behavior of azo dye by inactive CMC immobilized *Aspergillus fumigatus* beads. *Bioresour. Technol.* **2008**, *99*, 794–800.
(23) Gant, V.; Rodway, S.; Wyatt, J. Artificial neural networks: practical considerations for clinical application. In *Clinical Applications of Artificial Neural Networks*; Dybowski, R., Gant, V., Eds.; Cambridge University Press: New York, 2007.
(24) Chow, T. W. S.; Cho, S. *Neural Networks and Computing: Learning Algorithms and Applications*; Imperial College Press: London, 2007.
(25) Ripley, B. D. *Pattern Recognition and Neural Networks*; Cambridge University Press: Cambridge, 1996.
(26) Haykin, S. *Neural Networks: A Comprehensive Foundation*; Macmillan College (IEEE Book Press): New York, 1994.
(27) Hagan, M. T.; Menjah, M. Training feedforward networks with the Marquardt algorithm. *IEEE Trans. Neural Networks* **1994**, *5*, 989–993.
(28) Montgomery, D. C.; Runger, G. C. *Applied Statistics and Probability for Engineers*; Wiley: New York, 2003.